^{7}Li NMR and ^{35}Cl, ^{81}Br NQR Study of Lithium Ion Conductor $LiAlX_4$ (X=Cl and Br)

Koji YAMADA,* Masakazu KINOSHITA, Kayoko HOSOKAWA, and Tsutomu OKUDA
Department of Chemistry, Faculty of Science, Hiroshima University, Kagamiyama, Higashi-Hiroshima 724
(Received July 27, 1992)

The dynamic behavior of $LiAlX_4$ (X=Cl and Br) was studied by means of ^{7}Li NMR and ^{35}Cl, ^{81}Br NQR spectroscopies. The motional narrowing processes of the ^{7}Li NMR due to Li^+ diffusion were observed above room temperature for single crystals of $LiAlX_4$. The activation energies for these processes were 43.4 and 42.1 kJ mol^{-1} for the chloride and bromide analogs, respectively. A stepwise decrease in the ^{7}Li NMR quadrupole splitting suggested that the Li nucleus sees time averaged electric field gradient (EFG) arising from several different sites. The modulation effect of Li^+ diffusion on the NQR relaxation times was detected only for $LiAlBr_4$ but not for the chloride analog.

The high ionic conductivity of $LiAlCl_4$ was first reported by Weppner and Huggins, and the conductivity was $1.2\times10^{-6}\Omega^{-1}$ cm^{-1} at 298 K.[1] From DC polarization measurements for a series of $MAlCl_4$ (M=Li, Na, and K), the conductivity was attributed to the motions of the alkali metal ions. Higher ionic conductivity is expected by replacement of the cation and/or anion or by introduction of a divalent cation to form vacancies in the crystal lattice. The translational jump of the alkali metals in $LiAlCl_4$ and $NaAlCl_4$ was also suggested by the premelting behavior detected by DSC and ^{27}Al NMR techniques.[2] However, for these compounds no alkali metal NMR has been reported.

The NMR technique, especially by monitoring the diffusing nuclei, provides us with useful dynamic information on solid electrolytes. ^{7}Li is one of the most promising nuclei for the NMR study, and ^{7}Li NMR has been performed for Li_3N, lithium substituted β-alumina, perovskite related oxides, etc.[3—10] In order to get dynamic information monitoring quadrupole nuclei ($I>1/2$), several different experimental techniques have been employed, including the measurements of linewidth, quadrupole splitting, and relaxation times (T_1, T_2, and $T_{1\rho}$) against temperature. The change in the linewidth (motional narrowing process), however, is normally masked by the rather large quadrupole splitting for the powdery sample.

In this work the temperature dependence of the ^{7}Li NMR linewidth was examined on a single crystal to estimate the motional correlation times separately from the quadrupole splitting. The temperature dependences of the quadrupole splittings were also examined using powdery samples. From these NMR parameters a possible diffusion path is discussed on the basis of available crystal structure data. Finally, the dynamic properties of solid $LiAlCl_4$ and $LiAlBr_4$ were examined by measuring the ^{35}Cl and ^{81}Br NQR spin-lattice relaxation times, and the effect of cation diffusion is discussed.

Experimental

Sample Preparation. In studying the phase diagram between LiX and AlX_3 (X=Cl and Br), Kendall et al. observed congruent melting compounds $LiAlCl_4$ and $LiAlBr_4$ having melting points at 143 and 178 °C, respectively.[11] Single crystals of these compounds could be obtained by the Bridgman–Stockbarger technique fusing together stoichiometric amounts of AlX_3 and LiX. $AlCl_3$ was purified by sublimation in vacuo, and $AlBr_3$ was purified by recrystallization from the melt before use. The sample of $LiAlCl_4$ was checked by comparing the powder X-ray diffraction pattern with the simulated one based on the reported structural data.[12,13]

^{7}Li NMR and ^{35}Cl, ^{81}Br NQR Measurements. Broadline ^{7}Li NMR was carried out at 16 MHz with a JEOL MW60 spectrometer using a cylindrical single crystal and a powdery sample. ^{35}Cl, ^{81}Br NQR were observed on Matec pulse spectrometers (Model 5100+515 and 5100+525), and the spin-lattice relaxation times were determined by a conventional pulse technique.

Results and Discussion

Motional Narrowing Process of ^{7}Li NMR for Single Crystal. In the case of ^{7}Li NMR, the perturbation energy arising from the quadrupole interaction is normally greater than that from the dipolar one. In the case of $LiAlCl_4$ the former is about 20 kHz, which is about an order-of-magnitude larger than the dipolar broadening at 300 K. Then the motional narrowing resulting from the averaging process of the dipolar field is observable only by a single crystal experiment. Typical single crystal spectra are shown in Fig. 1. Exact information of the quadruple interaction tensor with respect to the crystal axes is usually derived from the analysis of the angular dependence of the spectra about three mutual perpendicular axes (Volkoff method).[14] In this experiment, however, a single crystal was used to see only the motional narrowing process as a function of temperature. As Fig. 1 shows, the width of each absorption line changed drastically without changing its position. In the case of the first order quadrupole effect on the $I=3/2$ nuclei, a single crystal spectrum splits into three components having intensity ratio 3:4:3 centered at the Larmor frequency.[15] The positions of the satellite lines, $(-3/2\leftrightarrow-1/2)$ and $(1/2\leftrightarrow3/2)$, depend on the orienta-

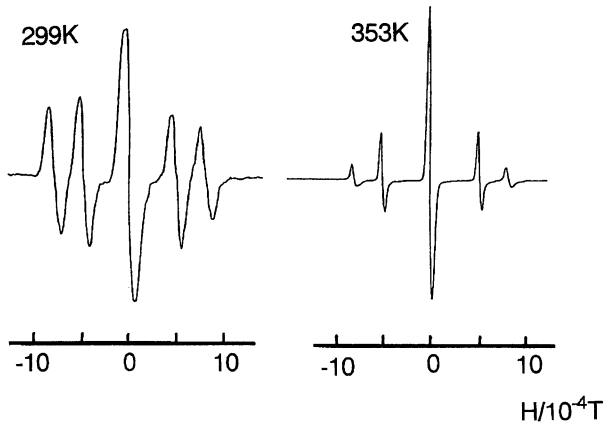

Fig. 1. Typical single crystal ^{7}Li NMR spectra of $LiAlCl_4$ at 16 MHz (H=0.9723 T). The crystal orientation was arbitrarily chosen so that to separate two sites having different EFG orientations.

tions of the quadrupole interaction tensors with respect to the external magnetic field. The presence of four satellite lines in Fig. 1 suggests that there are two crystallographically different orientations of the quadrupole interaction tensors consistent with the monoclinic system. In Fig. 2, the linewidths (defined as the peak-to-peak width of the derivative curve) of the central and satellite lines are plotted against temperature. The motional narrowing begins for all lines at about 280 K for $LiAlCl_4$. The linewidth of the central line at 390 K was only 0.1 Gauss (1 Gauss=10^{-4} T) as was expected from the self-diffusion process, and the narrowing limit was mainly caused by the instrumental effects such as field modulation and inhomogeneity. Using these central lines the correlation times, τ_0, for the corresponding motion were calculated by the following equation,[16]

$$\tau_0 = \tan[(\pi/2) \times (\Delta H^2 - B^2)/(A^2 - B^2)]/\alpha\gamma\Delta H, \quad (1)$$

where A, B, and ΔH are the linewidths below and above

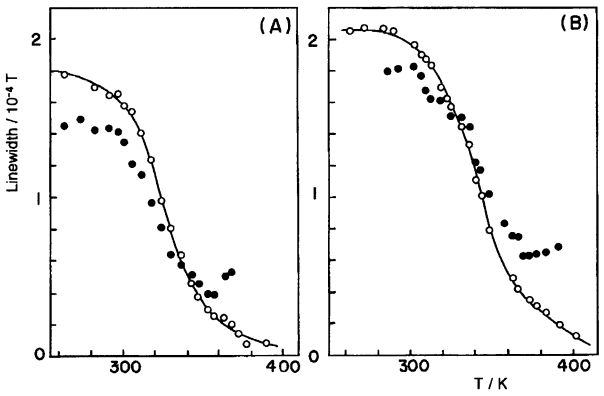

Fig. 2. Temperature dependence of the ^{7}Li NMR linewidth for (A) $LiAlCl_4$ and (B) $LiAlBr_4$. Solid curve indicates the calculated one using parameters listed in Table 1 assuming B=0 in Eq. 1. ○: Central line, ●: satellite line.

the motional narrowing temperature, and at the transition region, respectively. γ is the gyromagnetic ratio and α is a numerical constant around unity. In Fig. 3 the diffusional correlation times, determined by Eq. 1 assuming α=1, are plotted against inverse temperature. In these caluculations the linewidth at the narrowing limit, B, was assumed to be zero for both compounds because the temperature variations of the linewidths could be satisfactorily reproducible as shown by the solid curve in Fig. 2. The straight line in Fig. 3 corresponds to the Arrhenius type activation process expressed by

$$\tau_c = \tau_0 \exp(E/RT), \quad (2)$$

where E and τ_0 are the activation energy for the diffusional motion and the pre-exponential parameter, respectively. These parameters are summarized in Table 1.

The satellite lines show motional narrowing in the same temperature range, but they also show line broadening due to the ionic motion just below the disappearance temperatures (370 K for chloride and 400 K for bromide analog). A similar behavior was more clearly observed for Li_3N, where the motional line broadening was explained by ionic exchange between two crystallographically different sites with different electric field gradient (EFG) values.[6]

Just below the melting point, we were unable to detect new satellite line having a time averaged quadrupole splitting, though the motional correlation frequency is much higher than the quadrupole splitting ($(e^2Qq/h)/2<1/\tau_c$). This fact suggests that the Li^+ diffusion takes place not only through vacant Li sites but also through several interstitial sites as will be described

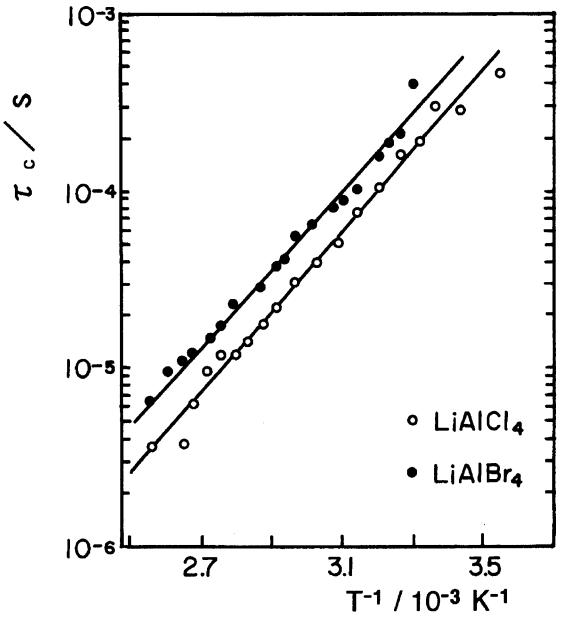

Fig. 3. Diffusional correlation times τ_c of Li^+ against inverse temperature.

Table 1. Dynamic Properties of $LiAlX_4$ Determined by ^7Li NMR and ^{35}Cl, ^{81}Br NQR

X	Method	E/kJ mol^{-1}	τ_0/s	b/s^{-1}	a/s K^2	n	Motional mode for E
Cl	^7Li NMR	43.4±3	5.5×10^{-12}				Li^+ diffusion[a]
	^{35}Cl NQR	95.6±3		5.0×10^{14}	2.31×10^{-5}	2.10±0.05	$AlCl_4^-$ reorientation
Br	^7Li NMR	42.1±3	1.5×10^{-11}				Li^+ diffusion
	^{81}Br NQR	41.5±3		4.1×10^8	1.05×10^{-3}	2.14±0.03	Li^+ diffusion

a) E=45.3 kJ mol^{-1} (from conductivity measurement).[1)]

later.

Temperature Dependence of the Quadrupole Splitting for a Powdery Sample. In contrast to the single crystal experiment, a stepwise change of the quadrupole splitting was detected using a powdery sample just below the melting point, as shown in Figs. 4 and 5. As described later, no phase transition was detected in both $LiAlCl_4$ and $LiAlBr_4$ because of the continuous temperature dependencies of the halogen NQR spectra from 77 K to their melting points. These findings suggest that the Li^+ ions begin to occupy several interstitial sites and the ^7Li nuclei see time averaged efg just below the melting point at which the diffusional correlation frequency is much higher than the quadrupole splitting. Hence the high ionic conductivity of these compounds is attributed to the intrinsic open structure of the crystal as was suggested by Chandra.[17)]

In order to find octahedral voids available in the crystal lattice, we estimated the volume and the EFG at several interstitial sites. The numerical calculation of the EFG was done according to the method reported by Nakayama et al.,[18)] in which the effect of cation diffusion was ignored. One of the possible interstitial sites considering the volume is (0, 0.5, 0.5) (=(0,0,0) from the symmetry operation) as shown in Fig. 6. Table 2 summarizes the calculated EFG and octahedral coordination around this site together with the Li^+ site. Although this site is octahedrally surrounded by six chlorine atoms similar to the Li^+ site, the sign of the EFG is inverse. The crystal structure of $LiAlCl_4$ can be described roughly as a hexagonal close-packed Cl^- anions in which a quarter of the octahedral voids and an eighth of the tetrahedral voids are occupied by Li^+ and Al^{3+} cations, respectively. Figure 6 shows the closed-packed Cl^- layers which correspond to the (202) plane. One of the possible diffusion paths is the zigzag chain through a void at (0, 0.5, 0.5) and the path is parallel to the b-axis. The numerically estimated $(e^2Qq/h)/2$ using the antishielding factor[19)] and the quadrupole moment were 110 kHz and −142 kHz for the Li and interstitial (0, 0.5, 0.5) sites, respectively. The former value is about six times larger than the observed one. However, the stepwise decrease of the quadrupole splitting could be qualitatively understood by assuming that the some fraction of the Li^+ occupies the interstitial sites with the jumping rate higher than the quadrupole splitting.

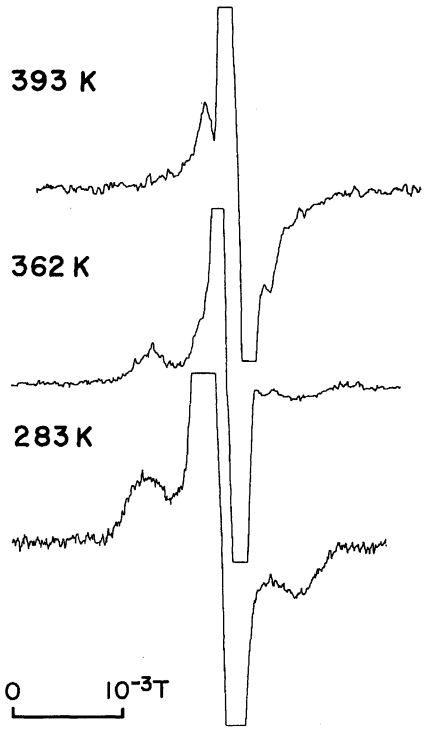

Fig. 4. Satellite line shapes of ^7Li NMR in the $LiAlCl_4$ powder sample at selected temperatures.

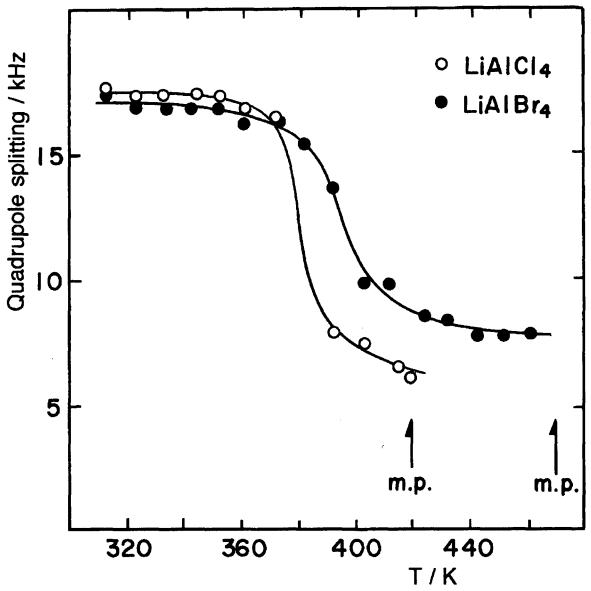

Fig. 5. Temperature dependence of quadrupole splitting, $(e^2Qq/h)/2$, for $LiAlCl_4$ and $LiAlBr_4$.

Table 2. Calculated EFG (q_{zz} and η) for the Li^+ Site and One of the Possible Intersticial Voids

Positional parameter	$q_{zz}/10^{20}$ J C^{-1} m^{-2}	η	Coordination
Li (0.1577, 0.985, 0.3646)	2.25	0.145	Octahedral by Cl atoms Li–Cl:2.475—2.841 Å
V (0, 0, 0)[a)]	−2.91	0.034	Octahedral by Cl atoms V–Cl:2.555—2.892 Å

a) Equivalent to (0, 1/2, 1/2) from the symmetry operation.

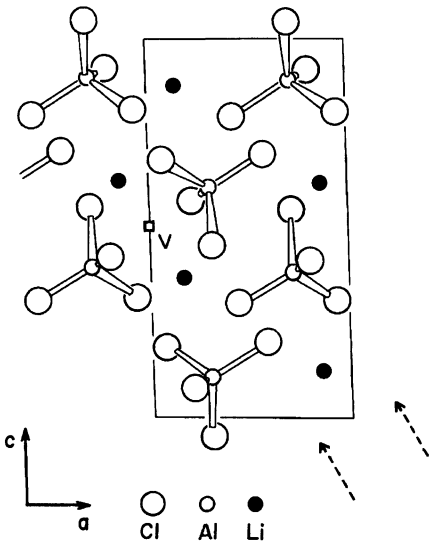

Fig. 6. Crystal structure of $LiAlCl_4$ projected on the *ac* plane. The arrow indicates the hexagonal packing layer parallel to the *b*-axis. One of the possible octahedral voids for translational diffusion is also shown.

It is interesting to evaluate the conductivity from our NMR data on the single crystal. In the simplest model one can estimate the ionic conductivity by the equation,

$$\sigma = Ne^2l^2/kT\tau_c, \quad (3)$$

where N is the concentration of the conduction ions, e is the charge on Li^+, and l is the length of the elementary jump. As a rough estimate we take a half of Li^+–Li^+ distance for l, we get $\sigma = 1.5\times10^{-7}\Omega^{-1}$ cm^{-1} at 298 K. This value is an order-of-magnitude smaller than the previously reported conductivity ($1.2\times10^{-6}\Omega^{-1}$ cm^{-1}).[1)]

^{35}Cl and ^{81}Br NQR of $LiAlX_4$ (X=Cl and Br). Both compounds showed four ^{35}Cl or ^{81}Br NQR lines in a temperature range between 77 and 400 K. Despite the cation diffusion above room temperature, there was no anomalous behavior in the temperature dependence of the NQR spectra. Table 3 summarizes the NQR frequencies for $LiAlX_4$. However, above room temperature, exponential decreases of the NQR relaxation times against temperature were observed for both compounds as shown in Fig. 7, in which linear portions of their low temperature sides show the contributions from the Raman process ($1/T_1$ is proportional to T^n, $n\fallingdotseq2$).

In general, the NQR relaxation rate $(1/T_1)_{obsd}$ is ex-

Table 3. ^{35}Cl and ^{81}Br NQR Frequencies for $LiAlX_4$ (X=Cl and Br)

Compound		Frequency/MHz 77 K	295 K
$LiAlCl_4$	Cl(1)	12.524	12.205
	Cl(2)	11.317	11.149
	Cl(3)	10.869	10.665
	Cl(4)	9.917	9.881
$LiAlBr_4$	Br(1)	88.872	86.739
	Br(2)	81.957	80.571
	Br(3)	76.869	75.657
	Br(4)	71.427	71.169

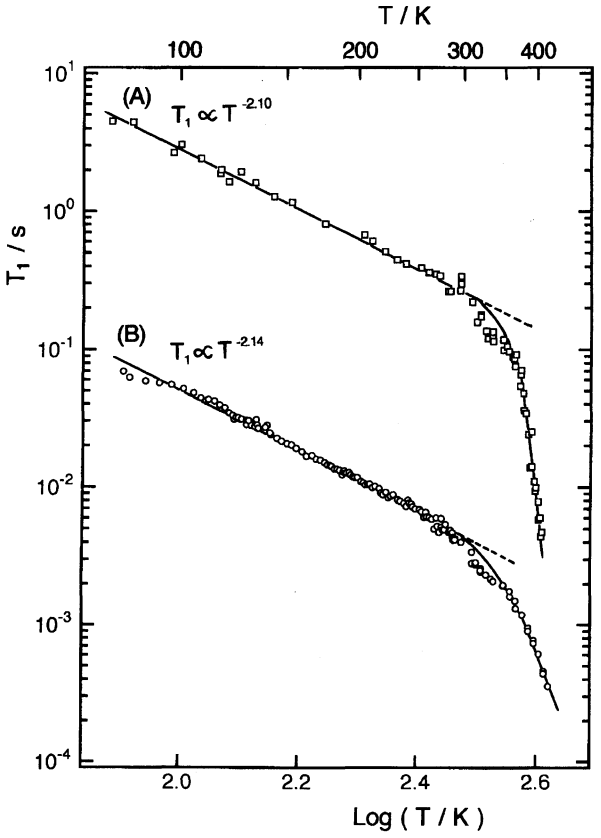

Fig. 7. Temperature dependence of ^{35}Cl and ^{81}Br NQR spin-lattice relaxation times for (A) Cl(2) in $LiAlCl_4$ and (B) Br(1) in $LiAlBr_4$.

pressed as a sum of the three contributions,[20—23]

$$(1/T_1)_{obsd} = (1/T_1)_{Raman} + (1/T_1)_{reor} + (1/T_1)_{mod} \quad (4)$$

where

$$(1/T_1)_{Raman} = aT^n \quad (5)$$

and

$$(1/T_1)_{reor} = b\exp(-E/RT). \quad (6)$$

The first term in Eq. 4 represents the Raman process and the second term is the contribution from the reorientation of the fragment containing nucleus monitored. The third contribution $(1/T_1)_{mod}$ is called the modulation effect arising from the EFG fluctuation nearby fragment and is expected to appear for these lithium ion conductors. According to Woessner and Gutowsky $(1/T_1)_{mod}$ is expressed as[21—23]

$$(1/T_1)_{mod} = (2/3)\omega_Q{}^2(q'/q)^2\tau_c/(1+\tau_c{}^2\omega_Q{}^2) \quad (7)$$

where ω_Q, (q'/q), and τ_c are the angular NQR frequency, fluctuation part of the EFG, and correlation time of the motion, respectively. In these $LiAlX_4$ compounds, τ_c for the Li^+ diffusion are numerically estimated from the NMR linewidth measurements and the relation $\tau_c\omega_Q \gg 1$ holds in the temperature range studied. Then Eq. 7 leads to

$$\begin{aligned}(1/T_1)_{mod} &= (2/3)(q'/q)^2(1/\tau_c) \\ &= (2/3)(q'/q)^2(1/\tau_0)\exp(-E/RT) \quad (8) \\ &= b'\exp(-E/RT), \quad (9)\end{aligned}$$

where $b' = (2/3)(q'/q)^2(1/\tau_c)$. Equation 9 is the same formula as Eq. 6. As Fig. 7 shows, we tentatively analysed the observed temperature dependence of the relaxation rate $(1/T_1)_{obsd}$ as a sum of the two terms,

$$(1/T_1)_{obsd} = aT^n + b\exp(-E/RT). \quad (10)$$

Relaxation parameters, a, n, b, and E for ^{35}Cl and ^{81}Br are summarized in Table 1. If $(1/T_1)_{reor}$ and $(1/T_1)_{mod}$ contribute to the relaxation competitively at the same temperature range, one can estimate the activation energy only for the process having higher activation energy. As Table 1 shows, the activation energy for the chloride corresponds to the $AlCl_4^-$ reorientation around the pseudo C_2 or C_3 axis because it is about two times larger than that of the Li^+ ion diffusion. For the bromide analogue, on the other hand, its value is in good agreement with that of the Li^+ diffusion.

The activation energy required for the AlX_4^- reorientation around pseudo C_3 or C_2 axis depends upon the site in the crystal lattice and the energy is roughly proportional to the temperature at which NQR signal disappears. For example, in the case of $AlBr_4^-$ reorientation in $AlBr_3 \cdot 2CH_3CN$ (which is described as $[AlBr(CH_3CN)_5]^{2+} \cdot 2AlBr_4^- \cdot CH_3CN$ in the crystal lattice), the ^{81}Br NQR signals assigned to the tetrahedral $AlBr_4^-$ anions disappeared at 240 and 300 K and the corresponding activation energies were determined to be 42 and 70 kJ mol^{-1}, respectively.[24] The activation energy for the $AlBr_4^-$ reorientation in $LiAlBr_4$ is estimated to be at least 80 kJ mol^{-1}, because ^{81}Br NQR signals could be still detected at 420 K. Therefore, we tentatively assign the deviation of the T_1 data from the Raman process above 300 K to the modulation effect of the Li^+ diffusion. At the same time, (q'/q) in Eq. 7 was estimated to be ca. 0.10, which is the same order as the previously reported values.[22,23] In the case of the chloride analog, the modulation effect could not be detected because in a similar temperature range the ^{35}Cl NQR relaxation in governed by the reorientation of the anion.

This work was partly supported by a Grant-in-Aid for Science Research on Priority Area of Organic Unusual Valence No. 03233102 from the Ministry of Education, Science and Culture.

References

1) W. Weppner and R. A. Huggins, *Phys. Lett. A*, **58A**, 245 (1976).
2) B. Krebs, H. Greiwing, C. Brendel, F. Taulelle, M. Gaune-Escard, and R. W. Berg, *Inorg. Chem.*, **30**, 981 (1991).
3) S. G. Bishop, P. J. Ring, and P. J. Bray, *J. Chem. Phys.*, **45**, 1525 (1966).
4) D. Brinkmann, W. Freudenreich, and J. Roos, *Solid State Commun.*, **28**, 233 (1978).
5) K. Differt and R. Messer, *J. Phys. C*, **13**, 717 (1980).
6) R. Messer, H. Birli, and K. Differt, *J. Phys. C*, **14**, 2731 (1981).
7) K. Kitahama, Y. Furukawa, S. Kawai, and O. Nakamura, *Solid State Ionics*, **3/4**, 335 (1981).
8) M. Villa, J. L. Bjorkstam, G. Mariotto, A. Fontana, and E. Cazzanelli, *J. Chem. Phys.*, **76**, 2804 (1982).
9) J. Senegas and M. Zriouil, *J. Solid State Chem.*, **58**, 137 (1985).
10) L. Latie, G. Villeneuve, D. Conte, and G. Le Flem, *J. Solid State Chem.*, **51**, 293 (1984).
11) J. Kendall, E. D. Crittenden, and H. K. Miller, *J. Am. Chem. Soc.*, **45**, 963 (1923).
12) Von E. Perenthaler, H. Shulz, and A. Rabenau, *Z. Anorg. Allg. Chem.*, **491**, 259 (1982).
13) G. Mairesse, P. Barbier, and J. P. Wignacourt, *Acta Crystallogr., Sect. B*, **35**, 1573 (1979).
14) G. M. Volkoff, H. E. Petch, and D. W. L. Smellie, *Can. J. Phys.*, **30**, 270 (1952).
15) A. Abragam, "Principles of Nuclear Magnetism," Oxford University Press, Oxford (1961), p. 233.
16) A. Abragam, "Principles of Nuclear Magnetism," Oxford University Press, Oxford (1961), p. 456.
17) S. Chandra, "Superionic Solids," North-Holland Publishing Co., Amsterdam (1981), p. 22.
18) H. Nakayama, K. Saito, and M. Kishita, *Z. Naturforsch., A*, **45**, 375 (1990).
19) P. C. Schmidt, K. D. Sen, T. P. Das, and A. Weiss, *Phys. Rev. B*, **22**, 4167 (1980).

20) H. Chihara and N. Nakamura, "Advances in Nuclear Quadrupole Resonance," Vol. 4, ed by J. A. S. Smith, Heyden & Son Ltd., London (1980), p. 1.
21) D. E. Woessner and H. S. Gutowsky, *J. Chem. Phys.*, **39**, 440 (1963).
22) Y. Tai, T. Asaji, D. Nakamura, and R. Ikeda, *Z. Naturforsch., A*, **45**, 477 (1990).
23) I. A. Kjuntsel, V. A. Mokeeva, I. G. Shaposhnikov, and G. B. Soifer, *Z. Naturforsch., A*, **45**, 531 (1990).
24) K. Yamada, T. Okuda, and H. Negita, *Z. Naturforsch., A*, **41**, 230 (1986).